https://doi.org/10.15302/frontphys.2025.032202

RESEARCH ARTICLE

Phononic frequency comb in carbon nanotube mechanical resonators at very high frequency band

Nan Xu[1], Zi-Jian Zhang[2,3,4], Sheng-Jie Xue[1], Tong Li[1,5], Qiang Zhou[1,6], You Wang[5], Hai-Zhi Song[5], Ke Zhang[2,3,4], Konstantin Arutyunov[7], Xin-He Wang[2,3,4,†], Guang-Can Guo[1,8], Guang-Wei Deng[1,6,8,‡]

[1] Institute of Fundamental and Frontier Sciences, University of Electronic Science and Technology of China, Chengdu 610054, China

[2] Fert Beijing Institute, Beijing 100191, China

[3] MIIT Key Laboratory of Spintronics, Beijing 100191, China

[4] School of Integrated Circuit Science and Engineering, Beihang University, Beijing 100191, China

[5] Southwest Institute of Technical Physics, Chengdu 610041, China

[6] Key Laboratory of Quantum Physics and Photonic Quantum Information, Ministry of Education, University of Electronic Science and Technology of China, Chengdu 610054, China

[7] Tikhonov Moscow Institute of Electronics and Mathematics (MIEM), National Research University Higher School of Economics, Moscow 101000, Russia

[8] CAS Key Laboratory of Quantum Information, University of Science and Technology of China, Hefei 230026, China

Corresponding authors. E-mail: †xinhe@buaa.edu.cn, ‡gwdeng@uestc.edu.cn

Received August 1, 2024; accepted October 28, 2024

Supporting Information

Supplementary Note 1: Phononic frequency combs of single-mode mechanical resonator

We first generate PFC in a mechanical oscillator of CNT with only one resonant mode. The resonant frequency of the bottom gated CNT system can be adjusted in a wide frequency range. Here, the equation of motion is described as

$$\ddot{Q}_1 + \omega_1^2 Q_1 + 2\zeta_1 \dot{Q}_1 + \alpha_{FPU} A_{2,2} Q_2^2 + \beta_{FPU} A_{1,1,1} Q_1^3 = P_D \cos(\omega_D t), \quad (1)$$

$$\ddot{Q}_2 + \omega_2^2 Q_2 + 2\zeta_2 \dot{Q}_2 + \alpha_{FPU} A_{1,2} Q_1 Q_2 + \beta_{FPU} A_{2,2,2} Q_2^3 = 0. \quad (2)$$

We can get the solution by the Poincaré-Lindstedt (PL) [1] perturbation method.

$$Q_i = A_0 \cos(\omega_i t) + A_p \cos(\omega_i + p\Delta\omega)t. \quad (3)$$

It can be seen that we obtain a discrete phonon frequency comb with equal spacing due to parametric coupling. The time domain signal, frequency domain signal and phase transition of phonon frequency comb are shown in the figure below.

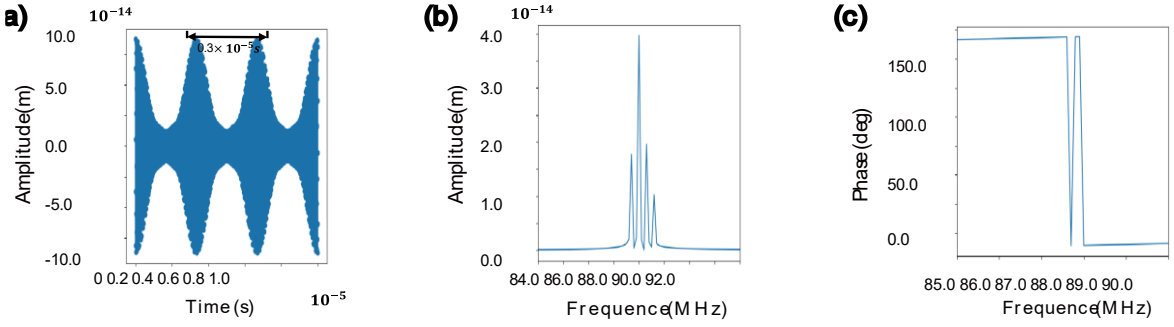

Fig. S1 Characteristics of single-mode phonon frequency comb. **(a)** Waveform corresponding to the output signal for the drive condition Sin=-25 dBm. **(b)** The displacement spectrum arranged in a comb-like pattern. **(c)** The phase transition corresponding to the phonon frequency comb.

In addition, we also discuss the conditions for the generation of parametric coupling and phonon frequency combs. Also under PL perturbation method, we apply the appropriate assumption of slow change envelope approximation to the equation of motion. By extracting the criterion from the deformed differential equation, we can obtain the conditions under which parametric coupling occurs and the conditions under which phonon frequency combs can be generated. The equations of dynamic are written as [2]

$$\ddot{Q}_1 + \omega_1^2 Q_1 + 2\zeta_1 \dot{Q}_1 + \alpha_{FPU} A_{2,2} Q_2^2 = P_D \cos(\omega_D t), \tag{4}$$

$$\ddot{Q}_2 + \omega_2^2 Q_2 + 2\zeta_2 \dot{Q}_2 + \alpha_{FPU} A_{1,2} Q_1 Q_2 = 0. \tag{5}$$

Existence condition for parameteric coupling:

The boundary conditions of PFCs are obtained by using the method of finding steady state points in slow dynamics. We assume the solution is $Q_i = \frac{1}{2}(u_i e^{j\omega_D t} + u_i^* e^{-j\omega_D t}),\ i = 1,2.$ We provide two first-order differential equations that describe the normalized amplitudes of the two modes. And we collect the coefficients of $e^{j\omega_D t}$ in Eq. (4) and coefficients of $e^{j\frac{\omega_D t}{2}}$ in Eq. (5) to obtain the following equations:

$$\ddot{u}_1 + (2\zeta_1 + 2i\omega_D)\dot{u}_1 + \left((\omega_1^2 - \omega_D^2) + 2i\zeta_1\omega_D\right)u_1 + \alpha_{FPU} A_{2,2} \frac{u_2^2}{2} = P_D \cos(\omega_D t), \tag{6}$$

$$\ddot{u}_2 + (2\zeta_1 + i\omega_D)\dot{u}_2 + \left(\left(\omega_2^2 - \frac{\omega_D^2}{4}\right) + i\zeta_2\omega_D\right)u_2 + \alpha_{12} \frac{u_1 u_2^*}{2} = 0\ . \tag{7}$$

Here, $\tau = \zeta_1 t, F_D = \frac{\alpha_{FPU} A_{1,2}}{8\zeta_1^2\omega_D^2} P_D \cos(\omega_D t)$, $\zeta_{21} = \frac{\zeta_2}{\zeta_1}, \Delta_1 = \frac{\omega_D - \omega_1}{\zeta_1}, \Delta_2 = \frac{\omega_D - 2\omega_2}{2\zeta_2}, \psi_1 = \frac{\alpha_{\mathrm{FPU}} A_{2,2}}{4\zeta_1\omega_D} u_1,$ and $\psi_2 = \frac{\sqrt{\alpha_{\mathrm{FPU}} A_{2,2} \alpha_{\mathrm{FPU}} A_{1,2}}}{4\zeta_2\omega_D} u_2$. In the slow-changing field, we obtain the following equations by two transformations under condition $\frac{\partial\psi_1}{\partial\tau} \to 0,\ \frac{\partial\psi_2}{\partial\tau} \to 0,\ \left(\zeta_1 \frac{\partial}{\partial\tau}\right) \to 0, \left(\zeta_2 \frac{\partial}{\partial\tau}\right) \to 0$. And we can get

$$-if - (1 + i\Delta_1)\psi_1 + i\psi_2^2 = 0\ , \tag{8}$$

$$-(\zeta_{21} + i\Delta_2)\psi_2 + 2i\psi_1\psi_2^* = 0\ . \tag{9}$$

We get two sets of steady state points (ψ_{1L}, ψ_{2L}), (ψ_{1P}, ψ_{2P}):

$$\psi_{1L} = \frac{-f}{-i + \Delta_1}\ , \tag{10}$$

$$\psi_{2L} = 0\ , \tag{11}$$

$$\psi_{1P} = i\frac{-f + \psi_{2P}^2}{(1 + i\Delta_1)}\ . \tag{12}$$

By substituting Eq. (9), we get

$$-(\zeta_{21} + i\Delta_2)\psi_{2P} - 2\frac{-f + \psi_{2P}^2}{(1 + i\Delta_1)}\psi_{2P}^* = 0\ . \tag{13}$$

For real solutions of ψ_{2P}^2, the criterion must be non-negative. Hence, we get the conditions for the existence of parametric coupling $f \geq \frac{1}{2}|\zeta_{21}\Delta_1 + \Delta_2|$. Region above two black lines in Fig. S2 can lead to parameteric coupling.

Existence condition for PFC:

Now, by taking fluctuations around the stationary solutions we redefine the fields as

$$\psi_1 = \psi_{1P} + \delta\psi_1, \tag{14}$$

$$\psi_2 = \psi_{2P} + \delta\psi_2. \tag{15}$$

Here, the stationary solutions $\psi 1P$ and $\psi 2P$ satisfy eq. 5 and eq. 6 and therefore we have the following

$$-if - (1 + i\Delta_1)\psi_{1P} + i\psi_{2P}^2 = 0, \tag{16}$$

$$-(\zeta_{21} + i\Delta_2)\psi_{2P} + 2i\psi_{1P}\psi_{2P}^* = 0, \tag{17}$$

and modulations $\delta\psi 1$ and $\delta\psi 2$ can only grow in strength if λ is both real and positive. After applying the Routh-Hurwitz criterion [3] to analyze the stability of the linearized dynamics, we set: $\delta\psi_1 = b_1 e^{\lambda\tau}, \delta\psi_1^* = b_2 e^{\lambda\tau}, \delta\psi_2 = b_3 e^{\lambda\tau}, \delta\psi_2^* = b_4 e^{\lambda\tau}$. And we obtain

$$\frac{\partial\delta\psi_1}{\partial\tau} = -(1 + i\Delta_1)\delta\psi_1 + 2i\psi_{2P}\delta\psi_2, \tag{18}$$

$$\frac{\partial\delta\psi_1}{\partial\tau} = -(\zeta_{21} - i\Delta_2)\delta\psi_2 + 2i\psi_{1P}\delta\psi_2^* + 2i\psi_{2P}^*\delta\psi_1, \tag{19}$$

$$\frac{\partial\delta\psi_1^*}{\partial\tau} = -(1 - i\Delta_1)\delta\psi_1^* - 2i\psi_{2P}^*\delta\psi_2^*, \tag{20}$$

$$\frac{\partial\delta\psi_2^*}{\partial\tau} = -(\zeta_{21} - i\Delta_2)\delta\psi_2^* - 2i\psi_{1P}^*\delta\psi_2 + 2i\psi_{2P}\delta\psi_1^*. \tag{21}$$

And Eq. (18) can be rewritten as

$$\lambda^4 + c_1\lambda^3 + c_2\lambda^2 + c_3\lambda + c_4 = 0. \tag{22}$$

Here we construct Hurwitz matrix

$$\begin{bmatrix} 1 & c_2 & c_4 & 0 \\ c_1 & c_3 & 0 & 0 \\ \frac{c_1c_2 - c_3}{c_1} & c_4 & 0 & 0 \\ \frac{c_1^2 c_4}{c_1c_2 - c_3} - c_3 & 0 & 0 & 0 \\ \dots & 0 & 0 & 0 \end{bmatrix}. \tag{23}$$

We need to satisfy

$$c_1 \geq 0, c_2 \geq 0, c_3 \geq 0, c_4 \geq 0, \tag{24}$$

$$c_1c_2 - c_3 \geq 0, \tag{25}$$

$$c_3(c_1c_2 - c_3) - c_1^2 c_4 \leq 0. \tag{26}$$

We can get

$$|\psi_{2P}|^2 \geq -\frac{\gamma_{21}(1+\Delta_1^2)[1+\Delta_1^2+4\zeta_{21}(1+\gamma_{21})]}{4(1+\zeta_{21})^2(1+\Delta_1^2+2\zeta_{21}+2\Delta_1\Delta_2)}. \tag{27}$$

The boundary condition that forms PFCs $2\Delta_1\Delta_2 \leq -(1 + \Delta_1^2 + 2\zeta_{21})$ are finally obtained. It is shown in orange in Fig. S2.

In summary, the regions above the black lines in Fig. S2 (gray, orange, and blue regions) lead to the excitation of parametric coupling. The gray region in the middle is the dispersion region, where no PFC is generated. The orange regions lead to the excitation of PFCs. The conditions satisfied in this experiment are $\omega_2 < \frac{\omega_1}{2}$, the range of PFC obtained by experiment is consistent with above analysis.

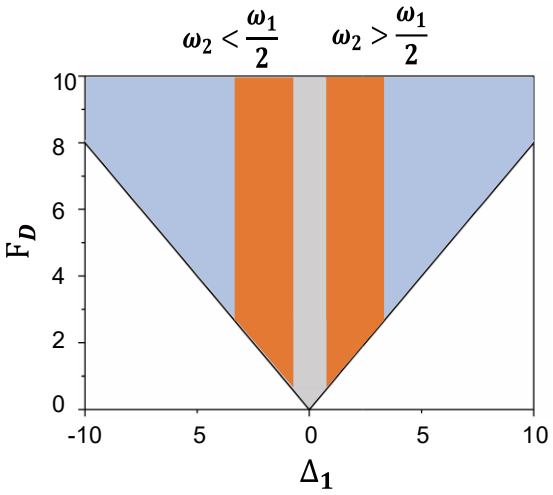

Fig. S2 Regions for parametric resonance (in blue), phononic frequency combs (in red) and dispersion band (in gray).

To verify the repeatability of the PFC, experimental tests were carried out in different mechanical CNT resonators. In a CNT system with different nonlinear degree, when the driving frequency and resonant frequency remain constant, we can find that the frequency comb lines increase with increase of the power.

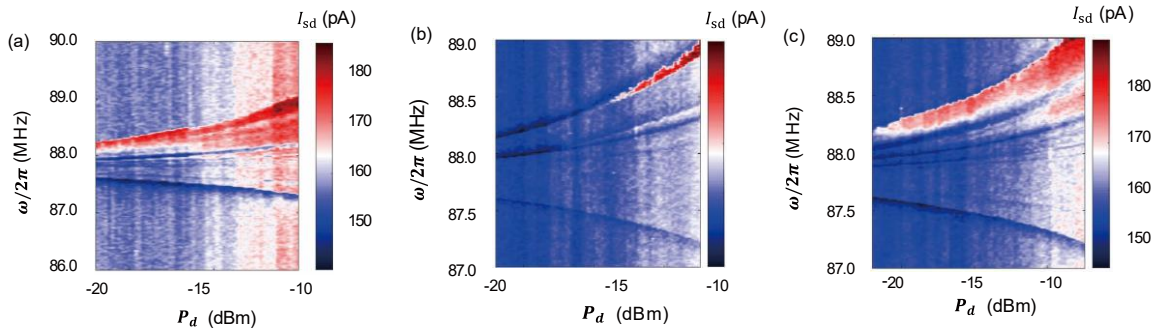

Fig. S3 Driving power dependence of the phonon frequency combs with constant gate voltage.

Supplementary Note 2: Phononic frequency combs of two-mode mechanical resonator

When there are two adjacent resonant modes in the carbon nanotube system, we can still see the phononic comb phenomenon near $\mathrm{RM_a}$ and $\mathrm{RM_b}$. Due to the interaction between the adjacent modes, the other resonant mode has obvious Duffing nonlinear effect. We can get the solution by the Poincaré-Lindstedt (PL) perturbation method. The equations of motion can be expressed as

$$\ddot{Q}_\mathrm{a} + \omega_\mathrm{a}^2 Q_\mathrm{a} + 2\zeta_\mathrm{a}\dot{Q}_\mathrm{a} + \alpha_{FPU} A_{\mathrm{a,b}} Q_\mathrm{a} Q_\mathrm{b} + \beta_{FPU} A_{\mathrm{a,a,a}} Q_\mathrm{a}^3 + \beta_{FPU} A_{\mathrm{a,b,b}} Q_\mathrm{a} Q_\mathrm{b}^2 = P_D \cos(\omega_D t). \tag{28}$$

$$\ddot{Q}_\mathrm{b} + \omega_\mathrm{b}^2 Q_\mathrm{b} + 2\zeta_\mathrm{b}\dot{Q}_\mathrm{b} + \alpha_{FPU} A_{\mathrm{a,b}} Q_\mathrm{a} Q_\mathrm{b} + \beta_{FPU} A_{\mathrm{b,b,b}} Q_\mathrm{b}^3 + \beta_{FPU} A_{\mathrm{a,a,b}} Q_\mathrm{b} Q_\mathrm{a}^2 = P_D \cos(\omega_D t). \tag{29}$$

Our equations consider both second-order and third-order nonlinearities. We need to make the nonlinearity and fluctuation occur simultaneously in the perturbation scheme. So we multiply Eq. (28) and Eq. (29) by ε. And we introduce a new variable:

$$\tau = \omega t. \tag{30}$$

So equations become

$$\ddot{Q}_\mathrm{a} + \omega_\mathrm{a}^2 Q_\mathrm{a} + 2\varepsilon\zeta_\mathrm{a}\dot{Q}_\mathrm{a} + \varepsilon\alpha_{FPU} A_{\mathrm{a,b}} Q_\mathrm{a} Q_\mathrm{b} + \varepsilon\beta_{FPU} A_{\mathrm{a,a,a}} Q_\mathrm{a}^3 + \varepsilon\beta_{FPU} A_{\mathrm{a,b,b}} Q_\mathrm{a} Q_\mathrm{b}^2 = \varepsilon P_D \cos(\omega_D t), \tag{31}$$

$$\ddot{Q}_{\mathrm{b}} + \omega_{\mathrm{b}}^2 Q_{\mathrm{b}} + 2\varepsilon\zeta_{\mathrm{b}}\dot{Q}_{\mathrm{b}} + \varepsilon\alpha_{FPU}A_{\mathrm{a,b}}Q_{\mathrm{a}}Q_{\mathrm{b}} + \varepsilon\beta_{FPU}A_{\mathrm{b,b,b}}Q_{\mathrm{b}}^3 + \varepsilon\beta_{FPU}A_{\mathrm{a,a,b}}Q_{\mathrm{b}}Q_{\mathrm{a}}^2 = \varepsilon P_D\cos(\omega_D t). \quad (32)$$

The most important of these are the small parameters expressed as differences with respect to τ and ε. We assume that

$$Q_a(\tau) = q_0(\tau) + \varepsilon q_1(\tau) + \varepsilon^2 q_2^2(\tau) + \cdots, \quad (33)$$

$$Q_b(\tau) = q_0'(\tau) + \varepsilon q_1'(\tau) + \varepsilon^2 q_2'^2(\tau) + \cdots, \quad (34)$$

$$\omega_a = \omega_0 + \varepsilon\omega_1 + \varepsilon^2\omega_2^2 + \cdots, \quad (35)$$

$$\omega_b = \omega_0' + \varepsilon\omega_1' + \varepsilon^2\omega_2'^2 + \cdots. \quad (36)$$

Bringing Eq. (33) back to Eq. (31), we obtain

$$\ddot{q}_0 + \omega_{\mathrm{a}}^2 q_0 = 0, \quad (37)$$

$$\ddot{q}_1 + \omega_a^2 q_1 = -2\varepsilon\zeta_{\mathrm{a}}\dot{q}_0 - \alpha_{FPU}A_{\mathrm{a,b}}q_0\mathrm{q}_0' - \beta_{FPU}A_{\mathrm{a,a,a}}q_0^3 - \beta_{FPU}A_{\mathrm{a,b,b}}q_0q_0'^2 + P_D\cos(\omega_D t). \quad (38)$$

The inter-modulation between drive tone and eigenmode is established through quadratic and cubic nonlinear terms and the tones $cos(\omega at)$ and $cos((\omega\mathrm{D} - \omega\mathrm{a})t)$ are produced in the frequency spectrum of $Q\mathrm{a}$. By solving equation though sequential iteration the coupling, the near-resonant terms of $cos((\omega\mathrm{a} + p(\omega\mathrm{D} - \omega\mathrm{a}))t); p \in Z$ are generated. The solution can be written as

$$Q_a = A_0\cos(\omega_a t) + A_p\cos(\omega_a + p\Delta\omega)\, t. \quad (39)$$

Similarly, by solving Eq. (32), we can also get near-resonant terms of $cos((\omega\mathrm{b} + p(\omega\mathrm{D} - \omega\mathrm{b}))t); p \in Z$.

Equally spaced discrete phonon frequency combs can be generated near both eigenmodes. The frequency domain signals are shown in the Fig. S4.

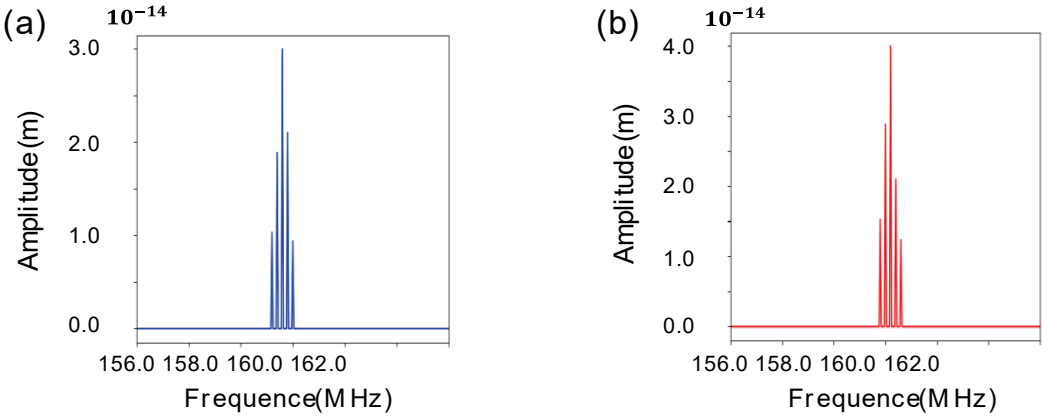

Fig. S4 Frequency response of phononic frequency combs near mode RM_a ($\omega_a/(2\pi)$=158.8 MHz) and mode RM_b ($\omega_b/(2\pi)$=159.1 MHz).

Here we briefly analyze the nonlinear coefficient of $\mathrm{RM_b}$. The coupled equations of motion in the presence of this potential become

$$\ddot{x} + \frac{\gamma}{m_{eff}}\dot{x} + \frac{k}{m_{eff}}x + \alpha x^3 = \frac{F}{m_{eff}}\cos(\omega_D t)\,. \quad (40)$$

In this equation, a mechanical oscillator with an effective mass of m_{eff} oscillates under the driving force of $F\cos(\omega_D t)$. x represents the amplitude, $\omega_2 = \sqrt{\frac{k}{m_{eff}}}$ represents the resonance frequency, and γ represents the damping coefficient. αx^3represents the first higher-order nonlinear term of the nonlinear response we are interested in Ref. [4]. We denote the nonlinear coefficients by α. In the case of our capacitance-coupled carbon nanotube mechanical oscillator, we use a simple DC measurement method. First, we apply a DC bias to the suspended CNT. The system's DC and AC signals are then applied to the bottom gate. The average electrostatic force on the resonator is then

$$F = \frac{1}{2}\frac{\partial C_g}{\partial x}(V_g^{DC} + V_g^{AC})^2. \tag{41}$$

Including C_g is at the bottom of the gate and the capacitance between the cavity, and depends on the number of elementary charges, capacitance, DC voltage V_{DC} will affect the tension of resonator, which may change the resonance frequency of the resonator. In addition, the gate voltage also controls the electrochemical potential of the quantum dot, as discussed in the text. The change in x is about displacement vibration $\delta x(\omega, t) = A(\omega)\cos(\omega_D t + \phi)$. And ω_D is the circular frequency that drives the AC signal, from which the phase difference drives the field $\delta V_g^{AC} = V_g^{RF}\cos(\omega_D t)$ and vibration. When we apply a microwave driving field to the mechanical resonator, the periodic driving force $F = \frac{\partial C_g}{\partial z} V_g^{DC} \delta V_g^{RF}$ will effectively excite the mechanical vibration. When we substitute the F into the coupling equation above, we can find that

$$A(\omega) = \frac{\frac{\partial C_g}{\partial z} V_g^{DC} \delta V_g^{RF}}{m_{eff}} \times \frac{1}{\sqrt{(\omega_m^2 - \omega^2 + \frac{3}{4}\frac{\alpha}{m_{eff}} A(\omega)^2)^2 + \frac{\omega_m^2 \omega^2}{Q^2}}}. \tag{42}$$

is the amplitude of mechanical resonator considering being nonlinear under strong driving power [5]. In the text, we show a typical fit of the nonlinear coefficient as a function of the driving frequency. In the frequency window where phonon combs can be generated, the nonlinear coefficient increases first and then recovers.

References

1. J. D. Logan, Applied Mathematics, 2nd Ed., John Wiley & Sons, 1997
2. Z. Qi, C. R. Menyuk, J. J. Gorman, and A. Ganesan, Existence conditions for phononic frequency combs, *Appl. Phys. Lett.* 117(18), 183503 (2020)
3. B.C. Kuo, Automatic Control Systems, Prentice-Hall, New Jersey, 1995
4. A. Ganesan, University of Cambridge, 2018
5. G. W. Deng, D. Zhu, X. H. Wang, C. L. Zou, J. T. Wang, H. O. Li, G. Cao, D. Liu, Y. Li, M. Xiao, G. C. Guo, K. L. Jiang, X. C. Dai, and G. P. Guo, Strongly coupled nanotube electromechanical resonators, *Nano Lett.* 16(9), 5456 (2016)